



HAL
open science

An Ultrasonic Testbench for Emulating the Degradation of Sonar Performance in Fluctuating Media

G. Real, D. Habault, X. Cristol, J. P Sessarego, D. Fattaccioli

► **To cite this version:**

G. Real, D. Habault, X. Cristol, J. P Sessarego, D. Fattaccioli. An Ultrasonic Testbench for Emulating the Degradation of Sonar Performance in Fluctuating Media. *Acta Acustica united with Acustica*, 2017, 103 (1), pp.6-16. 10.3813/AAA.919028 . hal-02292280

HAL Id: hal-02292280

<https://hal.science/hal-02292280>

Submitted on 19 Sep 2019

HAL is a multi-disciplinary open access archive for the deposit and dissemination of scientific research documents, whether they are published or not. The documents may come from teaching and research institutions in France or abroad, or from public or private research centers.

L'archive ouverte pluridisciplinaire **HAL**, est destinée au dépôt et à la diffusion de documents scientifiques de niveau recherche, publiés ou non, émanant des établissements d'enseignement et de recherche français ou étrangers, des laboratoires publics ou privés.

An Ultrasonic Testbench for Emulating the Degradation of Sonar Performance in Fluctuating Media

G. Real^{1),2)*}, D. Habault¹⁾, X. Cristol²⁾, J.P. Sessarego¹⁾ and D. Fattaccioli³⁾

¹⁾ Laboratoire de Mécanique et d'Acoustique, Aix-Marseille Université, CNRS, Centrale
Marseille, 4 impasse Nikola Tesla, CS 40006 13453 Marseille Cedex 13, France.

²⁾ Thales Underwater Systems, 525 Route des Dolines, 06903 Sophia Antipolis, France.

³⁾ DGA Techniques Navales, avenue de la Tour Royale, BP 40915, 83050 Toulon Cedex, France.

*email: gaultier.real@fr.thalesgroup.com

Summary

A scaled experimental protocol, in a water tank, is proposed to mimic the effects of medium heterogeneities on underwater acoustic propagation. The procedure consists in transmitting an ultrasonic wave ($f = 2.25$ MHz) through a RAndom Faced Acoustic Lens (RAFAL) in order to induce a spatially fluctuating sound pressure field. A scaling process based on a dimensional analysis ensures the representativeness of the experiment, when compared to the fluctuations of a few kHz continuous waves in the ocean. The regimes of saturation and unsaturation are explored by tuning the statistical parameters of the RAFAL's output face, the signal frequency and the propagation distance in the water tank. The control and reproducibility of the measurements is therefore ensured. The influence of volume effects is especially studied, since the experiments were conducted in free field conditions. Results in terms of mutual coherence function (second-order moment) are presented ; a good agreement is found between the values of radii of coherence calculated using experimental and simulation data, as well as theoretical results. The evaluation of the complex pressure distribution highlights the relevance of the experimental scheme, since behaviors typical of the regimes of fluctuations (saturation and unsaturation) are found.

1 Introduction

This paper is dedicated to underwater sound propagation in an uncertain fluctuating medium. The fluctuations of the characteristics of a medium can have a strong impact on wave propagation. This effect has been extensively studied over the last decades, in various domains, such as optics [35], electromagnetism [23], seismology [31] and acoustics (in air and water) [12].

The general objective of our work is to develop and validate techniques to detect targets in perturbed oceans. It is well known that the perturbations on the wave propagation lead to a loss of efficiency of the detection techniques. Therefore there is a need for new techniques and processing which can overcome the effect of the fluctuations. These techniques must be validated under experimental conditions. That is why in our opinion it is essential to develop an experimental protocol in a water tank in which all environmental parameters are controlled. Furthermore the experiment must be as reproducible as possible.

Several types of studies of these phenomena in controlled environments such as laboratory water tanks can be found in the literature. An extensive review of the results obtained in these experiments is proposed by Dobbins [14]. For instance, heating thermistors were used to generate thermal turbulence while an acoustic signal propagated through the perturbed medium (air or water). They provided very interesting results in terms of intensity moment [2], amplitude

fluctuations [9, 34] or spatial [33] and time correlation [6]. However, they are not fully reproducible since they only allow to recover the statistical behavior of the induced fluctuations. We propose here a fully deterministic protocol.

Our experimental study was motivated by results obtained in adaptive optics. Spectacular advances in terms of enhancement of the resolution of detection techniques have been observed in this field applied to observational astronomy [25]. Experimental protocols have been developed in the optical wave propagation domain such as scaled experimental testbenches in order to reproduce the effect of the atmospheric turbulence under laboratory conditions. They provided helpful tools to develop, validate or discard adaptive signal processing techniques [22, 27, 37].

This idea partly followed some results presented by Booker [3] which studied the non-intuitive representativeness of perturbations induced by an “almost-2D” rough phase screen, compared to those induced by an extended 3D fluctuating medium. This analysis was applied successfully to directive Gaussian beams in [1], with the conclusion that such protocols may be representative of extended medium configurations, under some specific conditions, such as the continuity in rms phase fluctuations in both cases.

The aim of this paper is to present such a protocol along with some experimental results which are compared with numerical results in order to validate the experimental design.

The focus here is on the volume effects. No interfaces (like the sea surface or the seabed) are taken into account. In this configuration, internal waves were proven to be responsible for the sound speed deviations from the mean value observed in shallow and coastal waters [20]. Let us point out that a protocol allowing to mimic the induced typical statistical features of the received signals is sought out, rather than the reenactment of the phenomenon responsible for the signal distortions.

The experimental design described in this paper consists in transmitting an ultrasonic wave through an acoustic slab of small thickness placed in a water tank. The output face of the slab, that is on the hydrophone side, is one realization of a randomly rough surface. The statistical and geometrical parameters of the experiment are chosen in order that the perturbations induced in the medium can be similar to perturbations in a fluctuating ocean, provided correspondence rules involving statistics of the roughness, frequency and range of propagation.

A manufactured slab, characterized by a few statistical parameters, is used to reproduce the effects of 3D propagation in a fluctuating medium. One slab corresponds to one realization of the roughness parameter. The roughness of the output face induces refraction and diffraction of the acoustic wave, causing alternating focal points and shadow zones, which are typical of long-range propagation of sound waves through linear internal waves or phase shift and wavefront distortions, which usually occur at short ranges. The source is moved along horizontal and vertical axis in order to highlight various statistically independent regions of the slab ; independent realizations of the sound field propagated through the slab can hence be obtained. This leads to two advantages :

- for one configuration of source, receiver and slab, the experiment is deterministic and therefore can be controlled and reproduced ;
- for several positions of source, receiver and slab, the illuminated part of the slab varies and corresponds to several realizations of a same set of statistical parameters.

To obtain relevant comparisons between configurations studied in a water tank and real scale oceanic cases, it was necessary to find a way to tightly relate these two kinds of configurations. This is achieved through a dimensional analysis. This analysis is based on the use of two specific

parameters defined by Flatté [12] the strength parameter (Φ) and the diffraction parameter (Λ). The values of these parameters may be used to define three kinds of regime : unsaturated, partially saturated and fully saturated. The scaling analysis includes a third parameter, the ratio of the vertical and horizontal acoustic correlation lengths of the acoustic perturbations induced in the medium to the wavelength (L_z/λ). With these 3 parameters a correspondence can be obtained between the water tank experiment and a perturbed ocean. The studied oceanic configurations presented here correspond to the propagation of acoustic waves in the mid-frequency band (1 – 15 kHz) over distances of the order 1 – 10 km. They correspond to short times of propagation compared with the daily period of medium fluctuations so that the studied phenomena are considered spatially random but frozen in time.

This paper is organized as follows.

In Section 2, we present a short summary of the dimensional analysis. Section 3 describes the numerical computations developed to chose the parameters of the experiment and to validate the experimental results. The experimental procedure is presented in Section 4. The experimental and numerical results are presented and analyzed in Section 5. Comparisons are made for the second-order moments of the sound pressure as well as for the complex pressure distributions. Conclusions and perspectives are given in Section 6.

2 Scaling Procedure

The experimental scheme consists in transmitting an ultrasonic wave from a transducer through a vertical slab named RAndom Faced Acoustic Lens (called RAFAL in what follows) characterized by a plane input face and a randomly rough output face. This random roughness is chosen as a Gaussian normal process with a zero mean and a standard deviation ξ_0 . The acoustic field is recorded on a hydrophone which is moved along a vertical axis. It is expected that the experimental configuration would induce perturbations similar to the perturbations obtained in an oceanic case [29]. As explained previously, in order to make qualitative and quantitative comparisons of the statistical characteristics of the sound field obtained with the experiment in the water tank and for some realistic oceanic cases, a scaling analysis is developed. The main points are summarized in this section along with the details on the choice of the parameters of both slab and oceanic cases.

The approach is based on the use of the Λ and Φ parameters and the evaluation of the ratio of the correlation length of the acoustic field to the acoustic wavelength L_z/λ [35]. The main assumption is that it is possible with these three parameters to qualify and quantify the induced fluctuations.

In the oceanic case, these parameters depend on the signal frequency f_s , the propagation range R , the standard deviation of the sound speed fluctuations δc_0 as well as on the vertical and horizontal correlation lengths of these fluctuations (L_{V_s} and L_{H_s}) (see Table 1).

For the RAFAL, each configuration is described by geometrical and physical parameters, namely the standard deviation of the roughness amplitude ξ_0 , the vertical and horizontal correlation lengths of the roughness, respectively L_V and L_H , the signal frequency f and finally the distance x_{dist} between the RAFAL's average output face and the receiver (see Figure 1). Therefore the main step is to express the three parameters (Λ , Φ and L_z) in terms of these quantities. This is done by first computing an analytical approximation of the sound pressure p based on several approximations, mainly the parabolic approximation and the Integral Small

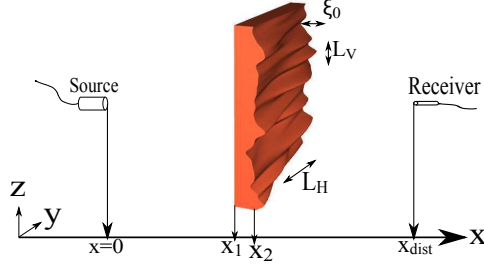


Figure 1: Experimental configuration diagram.

Table 1: Expression of the dimensional parameters for the oceanic case and the scaled experiment case.

Ocean	RAFAL
$\Phi^2 = k_0^2 \sqrt{2\pi} \left(\frac{\delta c_0}{c_0} \right)^2 L_{H_s} R$	$\Phi_\ell^2 = k_1^2 \xi_0^2 \left(1 - \frac{c_1}{c_2} \right)^2$
$\Lambda = \frac{R}{ak_0 L_{V_s}^2}$	$\Lambda_\ell = \frac{1}{2\pi} \left(\frac{R_F}{L_V} \right)^2$
$L_z = \alpha \lambda_s \frac{c_0}{\delta c_0} \left(\frac{L_{V_s}^2}{R L_{H_s}} \right)^{1/2}$	$L_z^\ell = \sqrt{\frac{\rho^2}{2q} + \frac{\left(\frac{x}{k_1} + \frac{b}{q} \right)^2}{\mathcal{R}}}$

Slope Approximation (ISSA)[36]. The evaluation of Λ_ℓ is based on the calculation of the Fresnel radius (obtained using its classical definition [4, 32]) and Φ_ℓ is obtained after analytical calculation of the average sound field $\langle p \rangle$. Finally, the vertical correlation length L_z^ℓ is obtained from the vertical intercorrelation function of p . The details of these calculations can be found in [28].

Table 1 summarizes the expressions of Λ , Φ and L_z/λ in typical oceanic configurations [12, 35] and in the experimental configuration. The acoustic wavenumber is defined as $k_i = 2\pi f/c_i$, where f is the signal frequency and c_i the sound velocity in medium i . The parameters which appear in this Table are defined as follows : a is a constant equal to either 2 in the case of a plane wave or 6 in the case of a point source, $\alpha = 0.24$, ρ is the transducer radius, $b = \frac{x_1}{k_1} + \frac{x_2 - x_1}{k_2}$, $d^2 = k_1^2 \xi_0^2 \left(1 - \frac{c_1}{c_2} \right)^2 \frac{1}{L_V^2}$, $q = 1 + \frac{d^2 \rho^2}{2}$ and $\mathcal{R} = \rho^2/8 + \frac{b^2 d^2}{1 + d^2 \rho^2/2}$.

Hence, the comparison is based on the equality between the three parameters in the ocean configuration and for the slab case [28, 29]:

$$\Lambda = \Lambda_\ell, \quad \Phi = \Phi_\ell, \quad L_z/\lambda_s = L_z^\ell/\lambda. \quad (1)$$

The $\Lambda - \Phi$ plane provides a way to relate each value of these two parameters to a corresponding regime of fluctuations :

- the unsaturated regime, where phase fluctuations mostly arise from the medium inhom-

geneities;

- the partially saturated regime, where correlated multipath propagation may be observed ;
- the fully saturated regime, where uncorrelated eigenrays are observed.

Of course, this is a global way to present the various regimes and in particular the two boundaries must not be understood as a strict separation, the regimes overlap in the transition zones (see Figure 2 for example).

3 Numerical Simulations

Numerical computations were conducted with two aims:

- to determine the parameters of the experimental configuration in relation with the parameters chosen for the oceanic cases
- to make comparisons of some of the statistical characteristics of the sound propagation for the slab and the ocean cases.

Once the statistical parameters of the RAFAL's output face were chosen, the propagation of acoustic wave through the designed RAFAL was tested through computer simulations. If the original set of parameters was validated by the simulation results coupled with the scaling analysis, the RAFAL is manufactured in order to correspond as much as possible to the model used in the simulations.

Two codes were used to compute the sound propagation through a RAFAL and to choose the parameters for the experimental configuration. One is called RAYTAL (for RAY Tracing through an Acoustic Lens) and is based on a ray tracing method. The other one is called P3DTE_x (for 3D Tank Experiment configuration) and is based on a 3D parabolic model.

In the computations, the directivity function of the source transducer was described as a plane circular piston ("Sombrero" function [21])[24]. This provides an accurate description of the radiation of the transducer used in the experiment. The source position is ($x_S = -0.2$ m; $z_S = 0$ m), the RAFAL's input plane face is located at $x = 0$ m and the average output face at $x = 0.02$ m.

As an example, Figure 2 presents a qualitative comparison of sound fields obtained with these two software, for one realization only (i.e. one profile and one source position) of RAFAL. The profile of the slab is shown on the left part of each figure. The calculation is carried out in 3D, but the propagation is observed on a plane orthogonal to the RAFAL which transverse section is drawn on the left of each figure. The sound levels are given following the color bar underneath. Figure 2 displays the acoustic pressure fields and ray beams for four configurations : the unperturbed case (a) that is the simple case where the acoustic slab presents two plane faces; the unsaturated (b), the partially saturated (c) and the fully saturated case (d). Figure 2 shows a good qualitative agreement between RAYTAL and P3DTE_x: the ray beams and high acoustic levels are superimposed. The unperturbed case points out the directivity of the transducer. Because the sound speeds in water and in the slab are quite close, the rays are not significantly refracted when propagating through the RAFAL. In the unsaturated case, a refraction of the ray beam is noticed. This result is confirmed by P3DTE_x. The resulting acoustic field is perturbed, but remains close to the result obtained in the unperturbed case. In the partially saturated case, there is a focalization of the acoustic field in the region ($x = 0.2$ m; $z = 0.01$ m), which is in agreement with the high acoustic amplitude computed with P3DTE_x. The fully saturated case

shows a large refraction of the rays and several focal points. These focal points lead to regions of high acoustic amplitude given by P3DTE_x.

All these results show that the propagation through a RAFAL does not simply result in a phase screen process but can produce 3D pressure fields similar to those obtained with volume effects. These qualitative observations are in good agreement with the comments found in the literature about sound waves propagation through a field of linear internal waves.

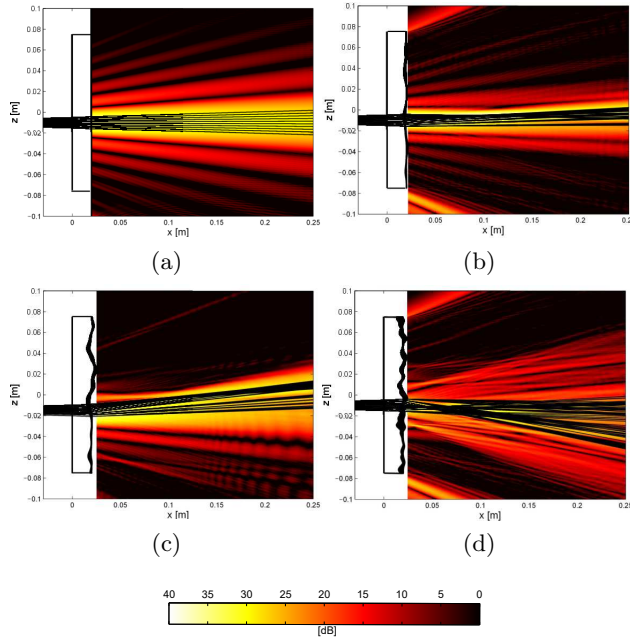


Figure 2: Simulation results: ray tracing programs & P3DTE_x - unperturbed case (a); unsaturated regime (b); partially saturated regime (c); fully saturated regime (d).

The third software P3DCOM (for Propagation in a 3D Corresponding Ocean) is also based on a 3D parabolic method and was used to compute the sound propagation in ocean [11]. It is used in the next sections to present more detailed comparisons between the slab case and the corresponding oceanic case.

4 The Experimental Procedure

4.1 The equipment

A diagram of the experimental set-up is given in Figure 3.

The measurements were conducted in a 3 m long, 1 m wide and 1 m deep water tank, filled with fresh water (see Figure 3). The temperature was continuously controlled by a probe so that the sound speed was accurately known at any time from the table in reference [13], assuming that its distribution is uniform inside the water tank. The dimensions of the slab are $15 \times 15 \times 0.2$ cm³. The equipment was located in the middle of the tank depth and it was possible to ignore the influence of the bottom and the surface.

The transmitted signal was a CW chirp at $f = 2.25$ MHz with a duration of $22.2 \mu\text{s}$ ($N_p = 50$ periods) and an amplitude of 5V. At this frequency and at a temperature of 20°C, the wavelength

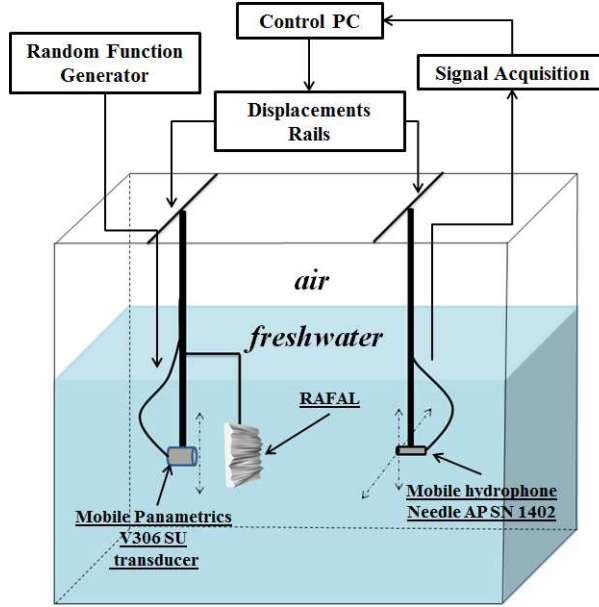


Figure 3: Experimental configuration.

λ is equal to 0.658 mm. The signal was generated with a *HP 33120A* Arbitrary Waveform Generator and sent through a *Panametrics V306* transducer (Figure 4) after $\times 10$ amplitude amplification by a *NF 4005* High Speed Power Amplifier.

The receiver was an *Acoustic Precision Needle* hydrophone (Figure 4). The signal was received on the control computer after high-pass filtering and amplification by a *Sofranel Pulse Receiver Model 5055PR*.

The acoustical equipment was placed on motorized rails driven by a computer interface (see reference [26] for more details). Automatic displacements of the source and the receiver allowed to provide several realizations for the same fluctuation regime and to carry out statistical studies. The measurements were repeated for several source depths in order to acoustically highlight several decorrelated regions of a RAFAL. In order for the realizations to be independent, the vertical displacement of the source was chosen to be equal to at least twice the vertical correlation length of the random roughness of the output face L_V . The number of RAFALs that needed to be manufactured was determined by the number of independent realizations available on a specific slab. The displacement of the hydrophone on a vertical axis was used to simulate vertical arrays of 64 hydrophones separated by a distance of 0.3 mm. This value was chosen in order to satisfy the sampling criterion ($s < \lambda/2$).

Table 2 summarizes the depth shifts between two positions of the source and the number of slabs that were manufactured. In the first column, FS, PS and US stand for Full Saturation, Partial Saturation and UnSaturation, respectively.

4.2 The RAFAL manufacturing process

The material chosen for the slabs is referred to as *Machinable Blue Wax* (used in reference [5]). Its physical properties were measured and are listed in Table 3. Its density is very close to the density in water so that they were assumed to be equal in the computations. Moreover,

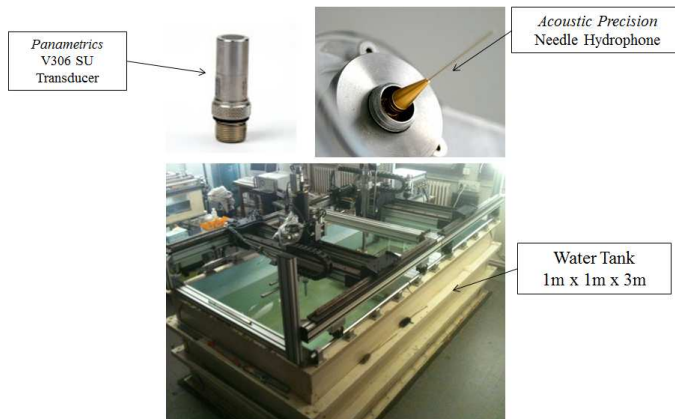


Figure 4: Experimental equipment - top left: Panametrics V306 SU transducer; top right: AP Needle hydrophone; bottom: water tank.

Table 2: Source depth shift Δ_{Z_s} , in mm, as a function of the vertical correlation length L_V , in mm. Corresponding number of realizations per RAFAL N_r and number of manufactured RAFALs per configuration N_{RAFAL} .

Config. #	L_V [mm]	Δ_{Z_s} [mm]	N_r	N_{RAFAL}
FS	4	10	22	2
PS	7	15	21	3
US	8	20	24	4

it was assumed that the propagation of shear waves could be disregarded since the shear wave attenuation was larger than 30dB/cm.

The manufacturing of the slabs was carried out in four steps.

Step one, the profile defined from the computations was interpolated and edited using a Computer Aided Design (CAD) software. In step two, the output file of the CAD software was sent to a 3D printer, producing a first version of the sample. However because of the temperature limitations of the 3D printer material it was not possible to directly use this sample.

Therefore, step three consists in using a molding silicone (RTV 2-RTV 123) in order to obtain a “negative” mold of the original profile. This silicone maintains its shape at high temperature. In step four the melted *Machinable Blue Wax* was poured in the negative mold. This last step was realized under the dome of an air pumping system in order to avoid the presence of air bubbles at the surface of the slab.

Figure 5 displays the RAFAL at the different steps of the manufacturing process [30].

Note that the design of these slabs is quite time consuming. Consequently, the number of RAFAL that could be manufactured was limited and it was not possible to acquire more experimental data.

5 Experimental Results

The experimental results are presented in this section. Comparisons between the measured data and the simulations are provided, first of all in terms of second-order moment of the pressure

Table 3: Measured physical properties - *Machinable Blue Wax*.

Density [g/cm ³]	$0.98 \pm 4.3 \cdot 10^{-5}$
Longitudinal Wave Sound Speed [m/s]	1975 ± 15
Shear Wave Sound Speed [m/s]	772 ± 16
Longitudinal Wave Attenuation at 2.25MHz [dB/cm]	13.1 ± 0.25

Table 4: Scaled experiment and corresponding oceanic medium parameters.

Config. #	$f = 2.25$ MHz			$f_s = 1$ kHz			
	ξ_0 [mm]	L_V [mm]	x_{dist} [mm]	δc_0 [m/s]	L_{V_s} [m]	L_{H_s} [m]	R [km]
1:FS1	2	4	250	0.77	31.9	106.3	19.9
2:FS2	2	4	150	1.04	19.9	199	5.89
3:FS3	2	4	100	1.99	14	140	2.26
4:PS1	2	7	150	1.46	23	230	2.58
5:PS2	2	7	125	1.88	20.2	202	1.78
6:US1	1	8	100	1.79	15.1	151.3	0.65
7:US2	1	8	50	2.24	12.4	247.5	0.25

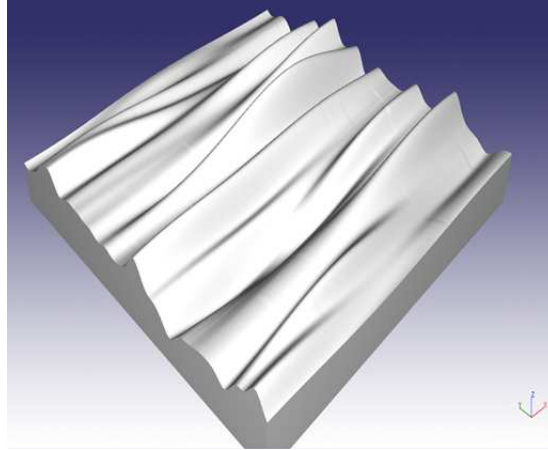
field, or mutual coherence function (MCF). Then, the complex pressure distribution (CPD), or phasor, is computed. The latter is used to retrieve the *a priori* classification of the experimental configurations in the various regimes of fluctuations.

5.1 Configurations studied

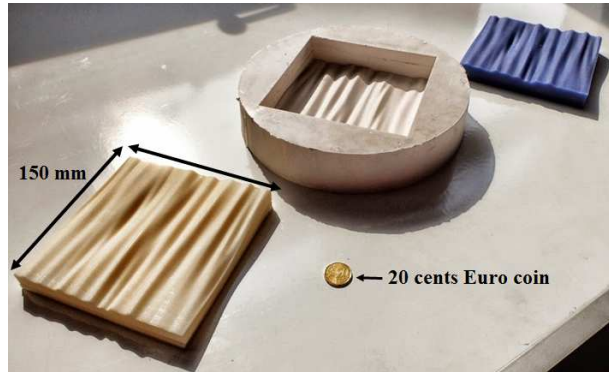
In order to be representative of realistic oceanic cases a set of 7 configurations was chosen from the procedure detailed in Section 2. They are shown in Table 4 where parameters for the tank experiment and the corresponding ocean configurations are listed.

As said previously the experiment was conducted for a $f = 2.25$ MHz frequency in the water tank. A frequency of $f_s = 1$ kHz was chosen for the corresponding oceanic configuration. This arbitrary choice was motivated by the fact that the P3DCOM software is definitely validated around this frequency.

The values of the parameters chosen for the oceanic cases are typical of what can be observed in the case of perturbations due to linear internal waves [12]. The standard deviation of the sound speed fluctuations is of the order of 1 m/s going from 0.77 m/s (FS1 configuration) to 2.24 m/s (US2 configuration). The values of the vertical correlation length of the sound speed fluctuations are also quite representative of what can be observed in oceanic media: from 12.4 m (US2) to 31.9 m (FS1). The ratio of vertical to horizontal correlation lengths of the sound speed fluctuations is a parameter that was tuned in order to obtain realistic results in terms of δc_0 . Nevertheless, this was performed taking into account the fact that the value of the horizontal correlation length of the sound speed fluctuations is typically of a few hundred meters. Here L_{H_s} lies between 106.3 m (FS1) and 247.5 m (US2). Finally, the range of propagation is also a critical parameter in an oceanic medium, since the saturation increases with the propagation distance (if the environmental parameters are the same). Here the parameter R spans from a few hundred meters ($R = 250$ m for US2) to more than ten kilometers ($R = 19.9$ km for FS1).



(a)



(b)

Figure 5: Manufacturing steps of the RAFAL - From left to right: CAD software (GLC) screenshot (step 1), 3D printer output (ABS) (step 2), negative mold (RTV2 - RTV123 Silicone) (step 3), final RAFAL (*Machinable Blue Wax*) (step 4).

Figure 6 represents the locations of the seven configurations in the $\Lambda - \Phi$ plane. From these results, two configurations were classified as fully saturated (FS1, FS2 and FS3), three as partially saturated (PS1, PS2) and two as unsaturated (US1 and US2).

5.2 Second-order moment of the pressure field

In this section, we compare the second-order moment (or mutual coherence function, MCF) obtained in various configurations. This function, denoted Γ , provides information on the correlation of the signal along a vertical linear array. The cross-spectrum matrix was first calculated and averaged over the whole number of realizations. The obtained quantity was then averaged over the iso-spaced sensors, leading to a function of the sensor spacing. More precisely, Γ is defined as [8, 10, 38]:

$$\Gamma(l) = \left\langle \left\langle \frac{\Pi(n) \Pi^*(n+l)}{|\Pi(n)| |\Pi(n+l)|} \right\rangle_{N_r} \right\rangle_N, \quad (2)$$

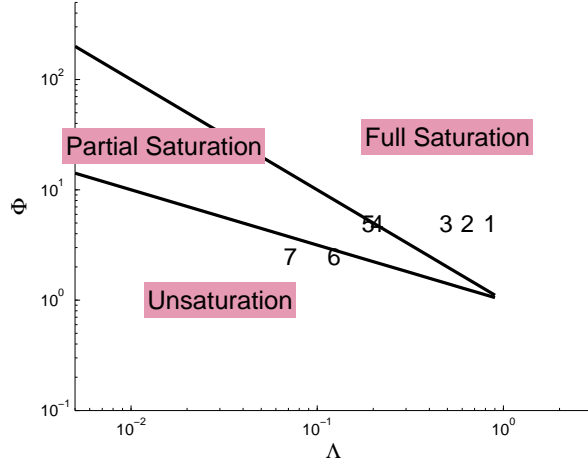


Figure 6: Experimental configurations in the $\Lambda - \Phi$ plane.

where l is the discrete sensor spacing, Π is the Fourier transform of the received signal, \cdot^* denotes the complex conjugate, $\langle \cdot \rangle_N$ is the ensemble average over the array (variable n) and $\langle \cdot \rangle_{N_r}$ is the ensemble average over the number of realizations.

Comparisons are made between the experimental results and the P3DTEX and P3DCOM results. Furthermore, they also include the theoretical solution given for the MCF by Collis et al [10] Flatté [12, 17, 19] where the MCF is approximated by an exponential function parameterized by the radius of coherence, denoted ρ_c in the continuous space domain and R_c in the discrete sensor spacing domain. Hence, the radius of coherence corresponds to the width of the main lobe of the second-order moment, denoted L_z in Section 2. The quadratic form of the phase-structure function is used [17]. The results associated with this formula will be referred to as simplified theory (ST) :

$$\Gamma^{ST}(l) = e^{-\frac{1}{2} \left(\frac{l}{R_c} \right)^2}. \quad (3)$$

Let us point out that this approximation of the MCF obviously provide the same value for the 3D fluctuating ocean and for the experiment because of the scaling procedure based on the same value of the normalized acoustic correlation length L_z/λ .

The comparisons obtained from the computations provide a tool to test the results obtained in the water tank. The idea that the MCF should behave differently depending on a specific regime of fluctuation is counterintuitive: the radius of coherence can sometimes be larger in a fully saturated case than in an unsaturated case. Therefore, it is not relevant to compare results obtained for different regimes. We emphasize on the fact that a consistency in terms of the evolution of the MCF as a function of the regime is sought out, rather than a perfect agreement between the different calculations: for instance, an increase (or a decrease) of the radius of coherence between two different configurations should be noticed with the simulation, experimental and theoretical results.

In the next paragraphs, the MCF functions are first presented for three configurations. They are displayed as functions of the sensor spacing normalized by the wavelength, s/λ , so that they can be compared for the scaled experiment and for the oceanic configurations Then a comparison

between radii of coherence is presented for the seven configurations.

5.2.1 MCF

The number of realizations used for each case is shown in Table 2. In Figure 7, $\Gamma(s/\lambda)$ is shown for 3 cases (each one corresponding to a specific regime). The experimental results and the P3DTE_x results are plotted with red circles and magenta diamonds respectively. When available, the P3DCOM results are plotted with cyan squares. The simplified theory is represented by a black solid line. Let us point out that P3DCOM could not be used for the unsaturated cases considered here because of the numerical spurious interference produced by the code at such very short distances ($R = 250$ m).

Figure 7a displays the MCF obtained for the US2 case. The MCF curves corresponding to the measurements and to P3DTE_x are in excellent agreement. Despite the fact that the number of realizations is much higher in the P3DTE_x case ($N_r = 240$, whereas in the measurements case, $N_r = 24$), the agreement for the main lobe of the MCF is quite good. Furthermore, the curve corresponding to the simplified theory is quite close to the other two.

Figure 7b presents the results obtained for the PS1 configuration. The agreement between the results provided by the scaled measurements, the numerical code (P3DTE_x and P3DCOM) and the simplified theory is still very good.

Figure 7c corresponds to the FS3 case. The number of realizations N_r is equal to 22 and equal to 220 for the P3DCOM and P3DTE_x computations. The agreement between the curves is still good overall, however some discrepancies appear. The experimental and the P3DTE_x curves are quite close but are different from the other two (simplified theory and P3DCOM) which are in good accordance.

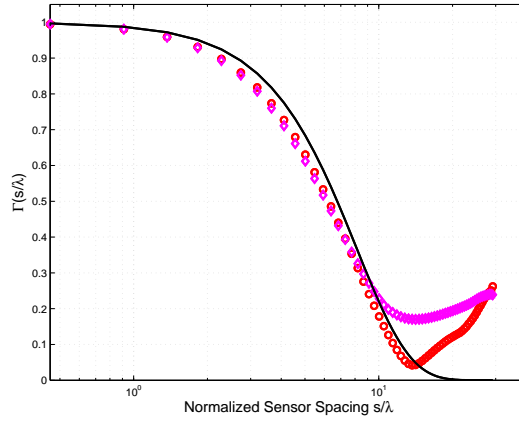
For the three configurations the experimental results and P3DTE_x are very close, although the number of realizations in the experimental case is quite low. This means that the experiment was conducted very carefully.

We observe a rise of the MCF “late secondary lobes” for large normalized sensor spacing in all cases. This is due to the fact that the value of the MCF as the spacing goes to infinity is given by $\Gamma(l \rightarrow \infty) = \left\langle \frac{\Pi(0)}{|\Pi(0)|} \right\rangle_{N_r} \left\langle \frac{\Pi(l)}{|\Pi(l)|} \right\rangle_{N_r}$ [12]. Although this value is statistically uncertain because of the small number of realization for the maximum sensor spacing, we can reasonably assume that is not 0, which is confirmed by the results in Figure 7. Nevertheless, the focus of our study is the estimation of the width of the first lobe and this secondary lobe could be easily suppressed by a windowing procedure.

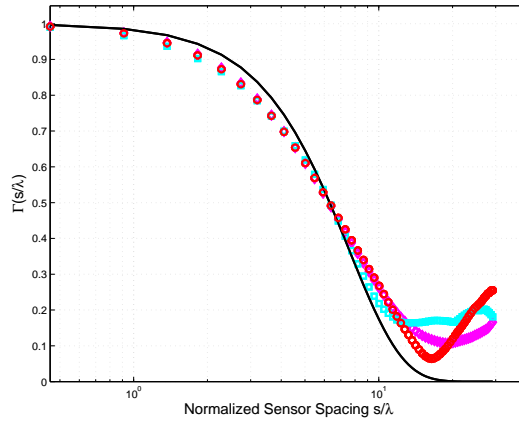
5.2.2 Radius of coherence

Other quantitative features to be investigated are the radii of coherence estimated from the numerical and experimental data. The radius of coherence is defined as the sensor spacing $s/\lambda = \rho_C$ such that $\Gamma(\rho_C) = e^{-\frac{1}{2}}$ [7].

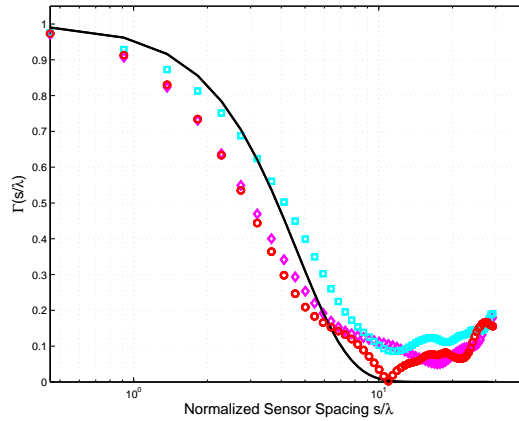
For each configuration located along the horizontal axis in Figure 8, 3 or 4 colored bars are presented. They correspond to the mean value of the radius of coherence obtained from each calculations (P3DTE_x, P3DCOM and simplified theory) and the experimental data. The error bars correspond to the standard deviation of calculations of the radius of coherence. For the experimental data, the error bars are not significant because of the rather small number of realizations. For the simplified theory, there is obviously no reason for error bars.



(a) US2 Configuration.



(b) PS1 Configuration.



(c) FS3 Configuration.

Figure 7: MCF - 64-sensor vertical linear array - Experimental data(\circ), P3DTEEx results (\diamond), P3DCOM results(\square), Simplified theory ($-$).

The analysis of Figure 8 confirms the conclusions already pointed out. The match between theoretical, simulated and measurements is quite good for most cases. As an example for the PS1 configuration the values for ρ_C are in excellent agreement since they vary from 5.05 to 5.35.

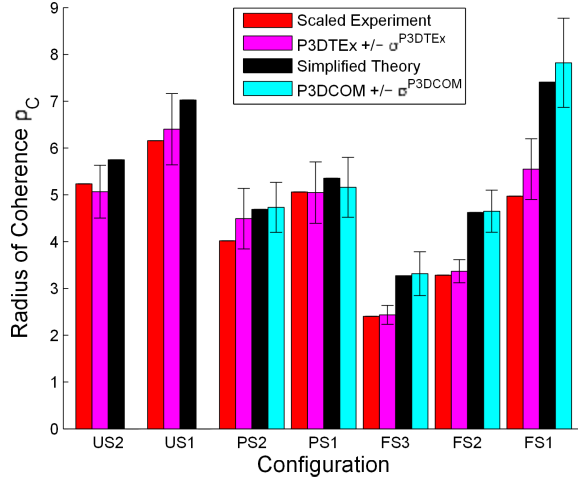


Figure 8: Comparison of radii of coherence ρ_C obtained with P3DCOM, experimental data, P3DTEx and simplified theory from left to right in all configurations.

Another example is given with the FS3 configuration, for which ρ_C is respectively equal to 3.31 for P3DCOM, to 3.27 for the simplified theory, and to 2.4 for the experimental case and for the P3DTEx calculation.

The general conclusion is that the theoretical solution and P3DCOM are in excellent agreement. Similarly, the scaled experiment and P3DTEx results are in remarkable concordance, but for some configurations there is a discrepancy between the two groups of results. The largest differences are obtained for the full saturation regimes.

It is interesting to notice the slight differences between the results obtained using the tank measurements and P3DTEx: the results are very similar, but the radius of coherence calculated in the simulation framework exceeds the scaled experiment radius in all cases. This may be explained by the uncertainty on several experimental parameters, for instance:

- the position of the hydrophone was estimated with an error of 0.1mm
- the plane input face of RAFAL could be not perfectly normal to the main axis of propagation although the orthogonality was measured by comparing time travels of signals reflected from various locations of the input face. Furthermore, slight local errors in the randomly rough face amplitude of the RAFAL are induced, due to the manufacturing process.
- the physical characteristics of the material composing the RAFAL were measured with uncertainties (see Table 3).

This could lead to possible differences between the results obtained with the experimental data and P3DTEx. However these differences are quite small.

The global comparison between the experiment and P3DCOM is quite satisfying but some differences appear. They obviously could be the result of too rough approximations made in the scaling procedure. The choice of the 3 parameters (Λ , Φ and L_V/λ) seems to be quite relevant. However a lot of approximations were used in order to evaluate the parameters for the slab case. For instance, the calculation of the sound pressure is based on the use of the ISSA which may not be valid for too high values of the RAFAL roughness. This is the case for the fully

saturated configurations which correspond to a large roughness amplitude and a small vertical correlation length. Some further computations must be conducted to evaluate the influence of such approximations on the accuracy of the parameters. If necessary, different approaches may be considered in order to derive the acoustic pressure field in the fully saturated configuration.

Let us remark also that the MCF obtained in the experimental framework (with RAFAL or P3DTEX) is slightly narrower than the theoretical approximation of the MCF. Similarly to what was explained earlier, this result can be explained by the approximations used to derive an expression for the theoretical radius of coherence in Section 2.

Finally, despite some discrepancies between the radii of coherence estimated in the fully saturated regime, the experiment provides very satisfying results. The fact that the measurements were conducted with great care should be highlighted. Moreover, although the number of realizations is much smaller in the experimental case than in the simulations configurations, the results are in good concordance, meaning that, for the MCF analysis, the number of realizations provided here is sufficient. In particular our main objective is fulfilled that is to reproduce perturbations of the sound propagation similar to those observed in a perturbed ocean. This means that this experiment is validated as a powerful tool to test detection techniques.

One aspect of the scaling procedure was therefore validated throughout this section (the L_V/λ parameter). Section 5.3 focuses on the validity of the other aspect of the procedure: the classification into regimes of fluctuations.

5.3 Complex pressure distribution

Another comparison between the experimental and numerical data may involve the behavior of the complex pressure distribution (CPD). Examples of CPD results can be found in [15, 18]. In the fully saturated regime, large phase and amplitude variations are noticed, inducing a chaotic representation of the so-called “phasor”. The CPD should therefore be concentrated in the zero area. In the unsaturated regime, the CPDs are distributed on the circle of mean complex pressure which corresponds to a variation of phase only. The partially saturated regime presents a transition between the other two.

Figure 9 displays CPD calculated on 16 hydrophones (corresponding to the 16 central sensors of the array) for 3 configurations. The real and imaginary parts of the complex pressure are displayed for each realization of the medium. They are normalized that is divided by the mean value of the pressure distribution for each configuration ($p_0 = \sqrt{\langle |p|^2 \rangle_{N_r}}$, plotted with the dashed line).

Let us first point out that the comparisons are mostly qualitative. The experimental results cannot accurately be analyzed because of the small number of realizations available. But the good comparisons done for the MCF prove that the numerical computations obtained with a larger number of realizations provide a correct simulation of the experiment.

Figure 9 presents the CPD for three cases (US2, PS1 and FS3, from left to right). For each one, the three lines respectively correspond to the experimental data, the P3DTEX and the P3DCOM computations.

The main features are globally similar to what was expected. Figure 9a, which depicts the US2 case, shows a CPD that tends to follow the mean complex pressure circle. A very good correspondence with the mean complex pressure is observed in all cases (Figures 9a, 9d and 9g). Figure 9c (FS3 case) shows that the CPD are relatively uniform but present numerous peaks

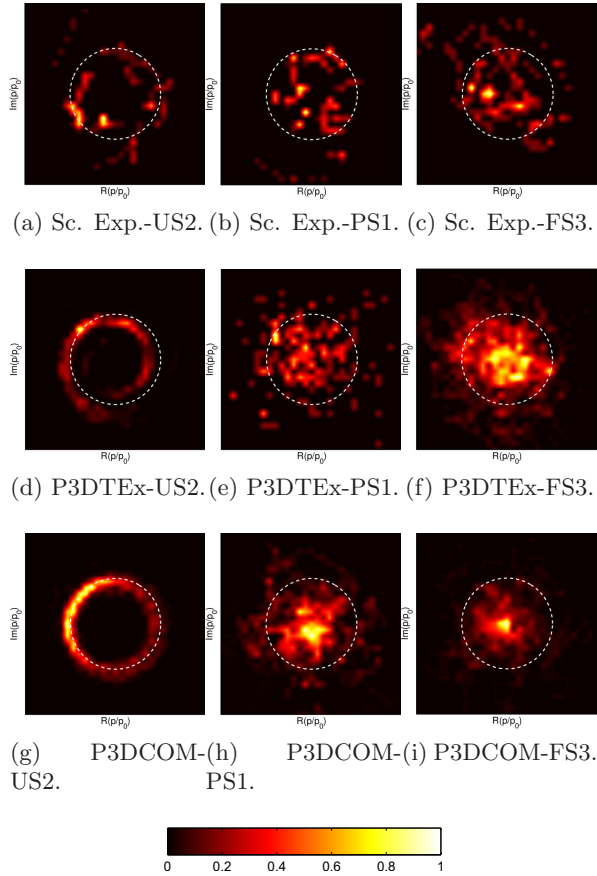


Figure 9: Complex pressure distribution (CPD) and mean complex pressure distribution (dashed circle) - Configurations (from left to right): US2, PS1 and FS3.

inside the mean pressure circle. Nevertheless, the P3DTEEx results enhances the analysis. The behavior of the phasor appears more clearly with an accumulation around the zero area in the FS3 configuration. As expected, the partially saturated case (PS1) appears as a transition between the FS3 and US1 configurations.

This analysis also applies to the results obtained using P3DCOM (third line), where the behaviors are extremely similar to the P3DTEEx values.

The CPD enhances the relevance of the scaling procedure in terms of regimes of fluctuations between oceanic environment and tank experiment setup.

6 Conclusions

This paper proposed an original approach to reproduce effects similar to those of internal waves on underwater acoustic propagation. Innovative corrective signal processing techniques could therefore be benchmarked using the data acquired in the water tank.

The experimental protocol consisted in propagating an ultrasonic wave through an acoustic slab. This procedure was carried out in a water tank in conditions such that scattering from the sea surface or the seabed were left aside. The manufacturing of the RAFAL, based on the use of a 3D printer and molding techniques, provide a tool to control the induced fluctuations

in a highly reproducible manner, which was, to our knowledge, not proposed before. It allows indeed to reproduce a given result for a given source-slab-receiver configuration faithfully and in a deterministic manner. The reproducibility of the procedure is to be highlighted since it permits to validate or discard several potential corrective detection techniques in the same experimental conditions.

A scaling procedure based on a dimensionless analysis provides a direct link between the experiment and oceanic scale observations. The acoustic data acquired in the water tank can hence be related to realistic at-sea configurations.

We provide in this paper a twofold data analysis. First, the mutual coherence function (MCF) was calculated for several configurations: using experimental data, parabolic equation simulations for the scaled experiment case and for the corresponding ocean medium case, and simplified theory. It remained consistent throughout the explored regimes of saturation and unsaturation. The estimation of the radius of coherence was proven to be accurate, which enhances the relevance of the experimental scheme from a quantitative degradation point of view. The deviations observed in the fully saturated regimes were analyzed and should not be attributed to experimental uncertainties. Nonetheless, a different approach may be needed to tackle the fully saturated case, because of the important roughness of the slab in this case. Second, the evaluation of the distribution of the complex pressure showed remarkably good behavior when compared to the available literature references. This reflects the relevance of the experimental protocol. Especially, it validates the *a priori* classification into qualitative regimes of fluctuations.

Overall the aimed phenomena were observed under laboratory conditions. Some improving paths may be explored, such as the use of receiver arrays, which would decrease the time necessary to conduct an experiment, and hence would allow for more realization to be processed. The manufacturing process theoretically presents no limitations and the studies conducted here should be extended to other spectrum of fluctuations than Gaussian only. The representativeness of other phenomena (turbulence, small-scale fluctuations due to sea surface agitation,...) could therefore be studied.

Also, an extensive analysis of the intensity fluctuations (fourth-order moment) of the data collected during the experiments will soon be available. It would however be interesting to provide a comparison between the results associated with the scaled experiment and real-scale data. The authors plan on using the data acquired during the ALMA [16] experiment to do so.

Acknowledgements

The authors would like to thank Régine Guillermin and Guy Rabau, as well as the staff from the SERM (mechanical technical support) at the LMA, for their help during the experiment. This work was sponsored by the Mission pour la Recherche et l'Innovation Scientifique (MRIS, DGA) and Thales Underwater Systems.

References

- [1] L.C. Andrews, R.L. Phillips, and A.R. Weeks. "Propagation of a gaussian-beam wave through a random phase screen". *Waves Random Media*, 7(2):229–244, 1997.
- [2] P. Blanc-Benon and D. Juvé. "Intensity fluctuations of spherical acoustic waves propagating through thermal turbulence". *Waves Random Media*, 3(2):71–83, 1993.

- [3] H.G. Booker, J.A. Ferguson, and H.O. Vats. “Comparison between the extended-medium and the phase-screen scintillation theories”. *J. Atmos. Terr. Phys.*, 47(4):381–399, 1985.
- [4] M. Brühl, G.J.O. Vermeer, and M. Kiehn. Fresnel zones for broadband data. *Geophysics*, 61(2):600–604, 1996.
- [5] D.C. Calvo, G. Canepa, R.J. Soukup, E.L. Kunz, J.-P. Sessarego, and K. Rudd. “Benchmarking of computational scattering models using underwater acoustic data from a corrugated wax slab”. *J. Acoust. Soc. Am.*, 123(5):3602–3602, 2008.
- [6] S.J. Campanella and A.G. Favret. “Time autocorrelation of sonic pulses propagated in a random medium”. *J. Acoust. Soc. Am.*, 46(5B):1234–1245, 1969.
- [7] W.M. Carey. “The determination of signal coherence length based on signal coherence and gain measurements in deep and shallow water”. *J. Acoust. Soc. Am.*, 104(2):831–837, 1998.
- [8] W.M. Carey, J.F. Lynch, W.L. Siegmann, I. Rozenfeld, and B.J. Sperry. “Sound transmission and spatial coherence in selected shallow-water areas: Measurements and theory”. *J. Comput. Acoust.*, 14(02):265–298, 2006.
- [9] N.P. Chotiros and B.V. Smith. “Sound amplitude fluctuations due to a temperature microstructure”. *J. Sound Vib.*, 64(3):349–369, 1979.
- [10] J.M. Collis, T.F. Duda, J.F. Lynch, and H.A. DeFerrari. “Observed limiting cases of horizontal field coherence and array performance in a time-varying internal wavefield”. *J. Acoust. Soc. Am.*, 124(3):EL97–EL103, 2008.
- [11] X. Cristol, D. Fattaccioli, and A.-S. Couvrat. “Alternative criteria for sonar array-gain limits from linear internal waves”. In *Proc. of the European Conference of Underwater Acoustics, Edimburgh, Scotland*, 2012.
- [12] R. Dashen, S.M. Flatté, W.H. Munk, K.M. Watson, and F. Zachariasen. *Sound transmission through a fluctuating ocean*. (Cambridge University Press), pp. 1-299, 2010.
- [13] V.A. Del Grosso and C.W. Mader. “Speed of sound in pure water”. *J. Acoust. Soc. Am.*, 52(5B):1442–1446, 1972.
- [14] P.F. Dobbins. *Degradation of Coherence of Acoustic Signals Resulting from Inhomogeneities in the Sea*. PhD thesis, University of Bath (UK), 1989.
- [15] L. Ehrhardt, S. Cheinet, D. Juvé, and P. Blanc-Benon. “Evaluating a linearized euler equations model for strong turbulence effects on sound propagation”. *J. Acoust. Soc. Am.*, 133(4):1922–1933, 2013.
- [16] D. Fattaccioli. “ALMA: a new experimental acoustic system to explore coastal waters”. In *Proc. of the 3rd Underwater Acoustic Conference, Chania, Greece*, pages 1–6, 2015.
- [17] S.M. Flatté. “Calculations of wave propagation through statistical random media, with and without a waveguide”. *Opt. Express*, 10(16):777–804, 2002.
- [18] S.M. Flatté. “Wave propagation through random media: Contributions from ocean acoustics”. *Proc. of the IEEE*, 71(11):1267–1294, 1983.

- [19] S.M. Flatté and G. Rovner. “Calculations of internal-wave-induced fluctuations in ocean-acoustic propagation”. *J. Acoust. Soc. Am.*, 108(2):526–534, 2000.
- [20] C. Garrett and W. Munk. “Space-time scales of internal waves”. *Geophys. Astro. Fluid.*, 3(1):225–264, 1972.
- [21] J.D. Gaskill. *Linear systems, Fourier transforms, and optics*. (Wiley New York), pp. 72-74, 1978.
- [22] S. Hippler, F. Hormuth, D.J. Butler, W. Brandner, and T. Henning. “Atmosphere-like turbulence generation with surface-etched phase-screens”. *Opt. Express*, 14(22):10139–10148, 2006.
- [23] A. Ishimaru. *Wave propagation and scattering in random media*, volume 2. (Academic press New York), pp. 346-375, 1978.
- [24] L.E. Kinsler, A.R. Frey, A.B. Coppens, and J.V. Sanders. *Fundamentals of acoustics*. (Wiley - VCH), pp. 180, 1999.
- [25] S.A. Metchev, L.A. Hillenbrand, and R.J. White. “Adaptive optics observations of vega: eight detected sources and upper limits to planetary-mass companions”. *Astrophys. J.*, 582(2):1102, 2003.
- [26] P. Papadakis, M. Taroudakis, F. Sturm, P. Sanchez, and J.-P. Sessarego. “Scaled laboratory experiments of shallow water acoustic propagation: Calibration phase”. *Acta Acust. United Ac.*, 94(5):676–684, 2008.
- [27] R. Rampy, D. Gavel, D. Dillon, and S. Thomas. “Production of phase screens for simulation of atmospheric turbulence”. *App. Optics*, 51(36):8769–8778, 2012.
- [28] G. Real. *An ultrasonic testbench for reproducing the degradation of sonar performance in random ocean*. PhD thesis, Aix-Marseille University, 2015.
- [29] G. Real, X. Cristol, D. Habault, J.-P. Sessarego, and D. Fattaccioli. “Rafal: RRandom Faced Acoustic Lens used to model internal waves effect on underwater acoustic propagation”. In *Proc. of the 3rd Underwater Acoustic Conference, Chania, Greece*, pages 1–6, 2015.
- [30] G. Real, J.-P. Sessarego, X. Cristol, and D. Fattaccioli. “De-coherence effects in underwater acoustics: scaled experiments”. In *Proc. of the 2nd Underwater Acoustic Conference, Rhodes, Greece*, pages 20–26, 2014.
- [31] H. Sato, M.C. Fehler, and T. Maeda. *Seismic wave propagation and scattering in the heterogeneous earth*. Springer, 2012.
- [32] F.W. Sears. *Optics*. Addison Wesley Publishing Company (not provided), 1949.
- [33] W.J. Sederowitz and A.G. Favret. “Covariance between acoustic signals traveling diverging paths in a random medium”. *J. Acoust. Soc. Am.*, 45(2):386–391, 1969.
- [34] R.G. Stone and D. Mintzer. “Transition regime for acoustic fluctuations in a randomly inhomogeneous medium”. *J. Acoust. Soc. Am.*, 38(5):843–846, 1965.

- [35] V.I. Tatarskii. *Effects of the Turbulent Atmosphere on Wave Propagation*. (National Technical Information Service, Springfield, VA), pp. 1-472, 1971.
- [36] A.G. Voronovich. *Wave scattering from rough surfaces*, volume 17. (Springer Science & Business Media), pp. 191-194, 2012.
- [37] C.C. Wilcox, J.R. Andrews, S.R. Restaino, and T. Martinez. “Atmospheric turbulence generator using a liquid crystal spatial light modulator”. In *Proc. of the Aerospace Conf.*, pages 1–8. IEEE, 2007.
- [38] D.K. Wilson. “Performance bounds for acoustic direction-of-arrival arrays operating in atmospheric turbulence”. *J. Acoust. Soc. Am.*, 103(3):1306–1319, 1998.